

Neural Shape-from-Shading for Survey-Scale Self-Consistent Bathymetry from Sidescan

Nils Bore & John Folkesson
Robotics, Perception and Learning Lab
Royal Institute of Technology (KTH)
Stockholm, SE-100 44, Sweden
Email: {nbore, johnf}@kth.se

Abstract—Sidescan sonar is a small and cost-effective sensing solution that can be easily mounted on most vessels. Historically, it has been used to produce high-definition images that experts may use to identify targets on the seafloor or in the water column. While solutions have been proposed to produce bathymetry solely from sidescan, or in conjunction with multibeam, they have had limited impact. This is partly a result of mostly being limited to single sidescan lines. In this paper, we propose a modern, salable solution to create high quality survey-scale bathymetry from many sidescan lines. By incorporating multiple observations of the same place, results can be improved as the estimates reinforce each other. Our method is based on *sinusoidal representation networks*, a recent advance in neural representation learning. We demonstrate the scalability of the approach by producing bathymetry from a large sidescan survey. The resulting quality is demonstrated by comparing to data collected with a high-precision multibeam sensor.

Keywords—Neural nets, Bathymetric maps, Sidescan, Data fusion, Representation learning

I. INTRODUCTION

Maritime area surveys are usually carried out using acoustic sensors. Because of the high attenuation of electromagnetic signals underwater, acoustic waves propagate significantly further at the same energy levels and therefore allow for longer range sensing. Among sonar types, sidescan and multibeam are most commonly used to survey larger seafloor areas. These two sensors exhibit some complementary properties, which leads to them often being used in conjunction. While multibeam returns three-dimensional positions, allowing for the creation of georeferenced height maps, sidescan only measures return backscatter intensities. Furthermore, sidescans are generally high-resolution compared to multibeam and have a wider swath range, thus surveying a larger area. The fine resolution of the sidescan can often be exploited by skilled sonar operators in order to detect objects on the seafloor.

While sidescan cannot be used to directly reconstruct geometry, it is clear that the signal does contain information about the slope of the seafloor. Indeed, a large portion of the signal can be well approximated by a Lambertian illumination model [1]. Because of

this, there has been several attempts at bathymetric reconstruction from sidescan images, most notably using shape-from-shading techniques [2]. All such methods inevitably face the problem of the sonar geometry. Sidescan emits a narrow beam along the direction of travel. However, the width orthogonal to this direction is very wide, resulting in the mentioned wide swath range. For each reflected intensity, the sensor measures only the two-way travel time, resulting in the angle of the recorded reflection being unknown. Typically, methods solve this by integrating the surface from a known or estimated point close to the vehicle in order to reconstruct the seafloor. However, even if the sonar is looking at a simple geometry such as a flat seafloor, it is difficult to model the sonar to such an extent that you can extract exact surface slopes. This results in the accuracy of the height estimate drifting the further away from the sensor you get.

Much like traditional shape-from-shading using real-world camera images, bathymetry reconstruction using single sidescan lines is an underconstrained problem. There is another line of research, often referred to as *inverse rendering*, that attempts to reconstruct a three-dimensional scene geometry using multiple calibrated camera images. With more images, it becomes tractable to pose this as an optimization problem, wherein a geometry is estimated that best reproduces all of the captured images. In recent years, that field has moved towards *differentiable rendering*, and more recently, neural networks as implicit representations of the three-dimensional geometry. This latter field of research is often referred to as *representation learning*, and neural models such as [3][4] produce state-of-the-art results. The differentiable nature of these models also present some tantalizing possibilities with regard to sidescan sonar. In particular, neural models such as [4] allow constraining the slope, or gradient, to match the one inferred from the sidescan intensity.

In order to reduce the impact of the estimate drifting when integrating the gradients, we propose also including some depth measurements. These may come from an altimeter echosounder or from bottom-tracking the sidescan signal itself [5]. The additional information greatly aids in the reconstruction as it allows the surface to be “pinned down” at certain points. In addition, we

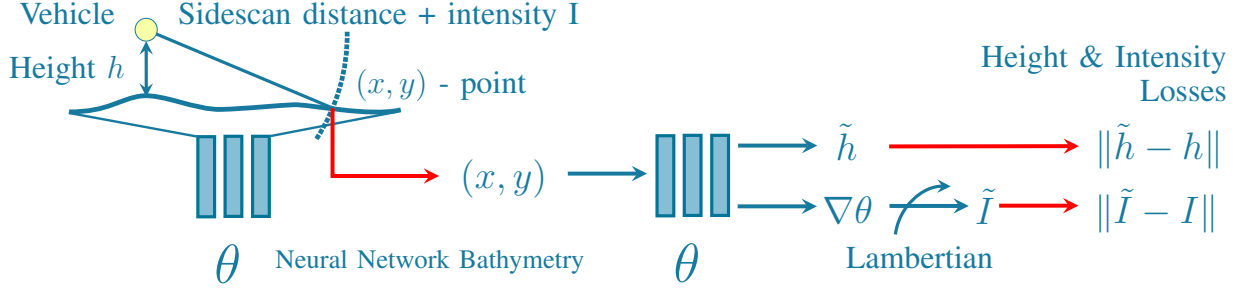


Fig. 1: Our method learns a bathymetry height map θ from sidescan intensities I and altimeter heights h . θ is a differentiable mapping from 2D x, y positions to seafloor heights h . When training, sidescan intensities are mapped to x, y points by finding intersections of isotemporal curves with the analytic representation θ . The method minimizes the distance to sparsely measured altimeter points h . From the gradient $\nabla\theta$, it also computes Lambertian intensities which are compared with the ground truth sidescan intensities. These aid the network in interpolating in between measured altimeter points.

argue that it is critical that bathymetry is predicted jointly from multiple sidescan lines at the same time. By phrasing it as a global optimization problem, and by employing recent computer vision advances, we can estimate the solution in a practical fashion. In doing so, the sidescan lines aid each other by reducing the uncertainty in seafloor height, thus letting the method focus also on reconstructing smaller scale detail such as rocks with high precision.

A method overview is illustrated in Figure 1. Our method receives as input sidescan intensities and ranges, as well as sparse depth measurements from an altimeter sensor. The bathymetry is represented as a neural network that maps two-dimensional positions to predicted heights. Since the representation is by its nature differentiable, it can also return surface gradients. With a simple Lambertian illumination model it can then generate predicted intensities that can be compared with the sidescan intensities. Indeed, since the intensities only put constraints on the gradient values, one can think of the model as optimizing a system of differential equations. The altimeter measurements provide the boundary conditions by allowing us to fix the solutions at some sparse points. Figure 2 illustrates the optimization procedure, starting from some random initial values.

We present the following contributions:

- 1) A novel, differentiable bathymetry representation
- 2) A framework for combining multiple sidescan lines into a self-consistent bathymetric model
- 3) Experiments that validate the scalability of the approach when applied to a large sidescan survey

A. Related work

Before discussing the problem of bathymetry estimation from sidescan, it will be instructive to first consider the inverse problem of simulating sidescan. As it is often simpler to reconstruct sidescan from bathymetry, this is

usually the way in which the former problem is phrased, with one notable exception being data-driven models [6]. Model-driven approaches [7] [8] [9] [10] [11] take as input seafloor geometry, possibly together with some relevant acoustic properties. They then “simulate” a sidescan by computing where the emitted beam could intersect the seafloor and reflect back in an amount of time corresponding to the temporal resolution of the sonar. The geometry as well as potential seafloor properties are used to reconstruct a signal. Most works assume some form of diffuse reflection model [12], with varying degrees of higher-order corrections added on top [7][8]. Again, there are examples of different, model-free approaches, including recent data driven models [13].

Many of the methods for solving the opposite, inverse, problem can be characterized as *shape-from-shading*. This technique was pioneered by Horn [14] to estimate geometry of diffusely reflecting materials from single camera images. Woodham [15] proposed a similar method with multiple calibrated cameras, alleviating reliance on the model assumptions being perfectly fulfilled. Langer & Hebert [16] were among the first to apply similar techniques to sidescan imagery. Similar to many subsequent methods, their method starts by removing any points corresponding to shadows, since they cannot be explained by the reflection model. In addition, they factor the reflection model into diffuse and specular components, similar to Jackson’s sonar model [7]. Dura et al. [9] compared Langer & Hebert’s method to calculating geometry through the inverse of Bell’s method [8]. In essence, since the latter is a linear operation on the Fourier transform of the sidescan signal, the inverse can be easily computed. They conclude that the two approaches are suitable in different scenarios, with their linear reflectance map approximation being more robust to noisy signals. Johnson & Hebert [17] provide a good overview of these early techniques for solving

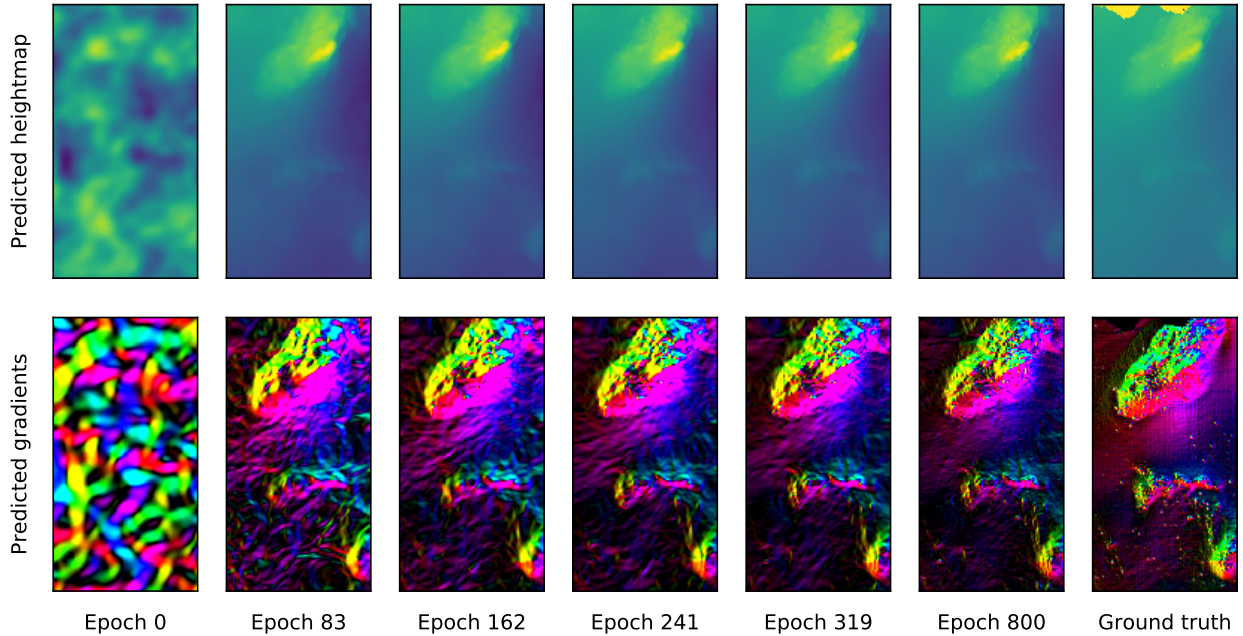


Fig. 2: Illustration of the progression of the training of our model, with height maps in the top row and corresponding gradients below. The model is initialized with random parameters. As training progresses, it quickly captures the large hill at the top of the image, as well as two smaller ones below. Around epoch 300, the model also starts to identify smaller rocks. At the far right, the corresponding ground truth bathymetry and gradients are presented.

the inverse problem. They propose an algorithm that augments the sidescan bathymetry with sparse direct bathymetric measurements. Specifically, they initialize the bathymetry estimate with the sparse measurements and perform a global optimization over imagery from one full survey line.

In a series of notable papers, Coiras et al. [2] [18] proposed a method to estimate not only the seafloor geometry, but also the surface albedo as well as the beam-pattern. Their method works solely from sidescan backscatter, and uses an expectation-maximization approach to alternately estimate these properties and then reconstruct the sidescan signal. To improve convergence, they gradually increase the resolution of the predicted bathymetry [18], with a lower resolution version used to initialize the next step. In particular, their results demonstrate the ability of the method to estimate all three properties realistically without significant overfitting to individual data points.

In one of the earliest systems for bathymetry-from-sidescan, Cuschier & Hebert [19] proposed an approach different from shape-from-shading. Their system identified shadows within the sidescan pings and used trigonometry to compute the height of the protrusions causing them. Similar to many subsequent shape-from-shading approaches, they then integrate the contributions from the individual slices to form the full seafloor profile. Notably, Bikonis et al. [20] combined shape-

from-shading with this sort of shadow information in order to extract improved depth estimates. In a conceptually similar but more elaborate approach, Woock & Beyerer [21] proposed deconstructing the sidescan signal into a “library” of signal templates, each with an associated bathymetry profile. By combining the contributing profiles, a full depth profile can then be reconstructed. While more complete than the simple shadow detection approach of [19], it faces similar challenges in reconstructing general types of seafloors. Recently, Jones & Traykovski [22] employed shadow geometry to reconstruct the surface surrounding a rotating sidescan mounted close to the seabed. They perform thorough evaluations of the efficiency of their method, with quantitative comparisons to multibeam bathymetry.

While many early works [19][16] focus on estimating geometry mostly from sidescan, they generally note that the problem is ill-defined without some additional assumptions or boundary conditions. Li & Pai [23] suggest a different route by augmenting multibeam data with sidescan. Their method works on a grid-based terrain model, with each grid cell forming the boundary of a shape-from-shading problem in between the multibeam points. With a typical high-resolution sidescan, the resolution of the terrain model can thus be enhanced. Johnson & Hebert’s approach [17] is more general in that it only relies on depth measurements wherever available. They optimize a local surface in

sidescan coordinates. The optimized surface is then used to associate the sidescan bins with grid cells in a global coordinate system. In the final step, the grid representation is optimized using a non-linear minimization technique similar to Horn’s [24]. The sparse depths are used to initialize the height map, but only smoothness regularization is used as a constraint. Johnson & Hebert’s approach [17] is notable in that it is *in principle* able to deal with observations originating from multiple sidescan lines. Most other methods for constructing aggregate bathymetric maps [25] [26] have not dealt explicitly with this problem. Instead, they have proposed forming submaps for different lines [25] or simply averaged the individual geometries [26].

Looking more generally at sonar geometry, several methods for reconstructing three-dimensional geometry from wide-aperture sonar have been proposed. As 2D imaging sonars cover a large volume with significant overlap in-between subsequent measurements, it is viable to use feature-based structure-from-motion [27][28] to estimate sensor motion as well as sparse geometry. To form dense object geometry, space-carving methods [29][30] may be used. However, they work poorly for non-convex geometries, including most seafloor geometries of interest. More recently, works such as [31] [32] [33] applied more detailed backscatter models, resulting in higher-quality reconstructions [31][33]. Guerneve et al. [33] suggested a method for resolving high-resolution surface structures from wide-aperture sonar by means of a spatially varying deconvolution approach. The method is fast but constrained to motion along the wide beam angle of the sonar (typically corresponding to the z-axis). To infer geometry from unconstrained motion, Westman et al. [32] proposed inferring an acoustic “albedo” field for the full surveyed volume, by means of a *non-line-of-sight* (NLOS) reconstruction. Since the field is a scalar field that is uniform in all directions, it does not take geometric surface scattering into account. A synthetic aperture tomography approach was also presented in [34]. The method extracts high-definition models of relatively small objects from data collected by an autonomous underwater vehicle equipped with a *synthetic aperture sonar* (SAS) sensor.

One important aspect that differentiates the surveyed methods is how they solve the optimization problem resulting from trying to reconstruct the backscatter. Dura et al. [9] characterize the early methods as either global optimization, propagation out from a known height or as linear approaches. The vast majority of later approaches [17] [18][20] [26][32] can be characterized as global optimization, meaning that they optimize the full ping or image jointly. The difference is often in the solution to the optimization problem, with methods using for example general non-linear solvers [17], sparse solvers [32] or expectation-optimization with gradient descent [18]. An advantage of global optimization is that priors such as smoothness on the produced bathymetry can be enforced, thus increasing robustness to sensor noise or modeling errors. So far, no method has been proposed

that utilizes the GPU-accelerated optimization of modern deep learning libraries.

Our method presents a scalable solution to the shape-from-shading problem from multiple sidescan lines. The mathematical model is similar to that of Coiras et al. [18]. However, we employ a neural network as the bathymetric representation, similar to recently proposed representation learning systems [4]. In contrast to [18], our method combines many sidescan lines into a self-consistent, georeferenced bathymetry. By optimizing all of the lines jointly using the GPU, their individual estimates can reinforce each other to remove some of the inherent ambiguity of the inverse problem. Our optimization scheme itself is somewhat similar to the reconstruction from forward-looking sonar described by Westman et al. [32]. An important advantage of our method is that our model incorporates the geometric backscattering through the incidence angle. Johnson & Hebert’s approach [17] is similar to ours in that it in principle allows for several sidescan lines, and also accommodates sparse depths. In contrast to that paper and all previous work, we demonstrate our method on many sidescan lines, from a large area survey, and jointly optimize the bathymetry to reconstruct all the backscatter data. In addition, we provide an extensive quantitative evaluation where we compare the produced bathymetric map to high-precision multibeam bathymetry.

B. Problem statement

The goal of the described method is to construct high-precision bathymetry from many sidescan survey lines together with some sparse depth measurements. We assume that the global pose of the sidescan and depth sensors are known, either through GPS or some other means of localization, such as *simultaneous localization and mapping* (SLAM).

II. METHOD

We begin by defining our bathymetric representation θ as well as the rather general loss terms that we use to optimize it. Subsequently, we will describe how to simulate sidescan observations given this bathymetric representation in a differentiable manner.

A. Loss functions

Our method aims to find a function $\theta : \mathbb{R}^2 \rightarrow \mathbb{R}$ that maps two-dimensional Euclidean world coordinates to the respective seafloor height. As will become clear, it is crucial that θ is differentiable. While θ could in principle be any trainable, differentiable black box method, we will take it to be an *multi-layer perceptron* (MLP) variant known as a *Sinusoidal Representation Network* (SIREN) [4]. The method has the advantage of giving high-quality derivatives, as well as not suffering from “spectral bias” [35]. The latter feature allows the network to also learn smaller, high-frequency, features of the seafloor.

Inputs	Description
$t_i \in \mathbb{R}^3$	sidescan origin at ping i
$\mathbf{R}_i \in SO(3)$	sidescan rotation matrix at ping i
$I_{i,n} \in \mathbb{R}$	intensity at ping i and time bin n
$p_j^{gt} \in \mathbb{R}^3$	measured seafloor height
Outputs	
$\theta : \mathbb{R}^2 \rightarrow \mathbb{R}$	bathymetry height map
$R : \mathbb{R}^2 \rightarrow \mathbb{R}_+$	albedo map
$\Phi : \mathbb{R} \rightarrow \mathbb{R}_+$	beam-pattern
A_i	per-line gain

TABLE I: The main inputs and outputs of our method.

Our method aims to reconstruct bathymetry from sparse altimeter readings, as well as dense sidescan imagery. In addition, for this study we rely on high-quality positioning, see Table I for all inputs to the method. We will therefore have two parts to our loss function, with α determining their relative importance,

$$\mathcal{L} = \mathcal{L}_\nabla + \alpha \mathcal{L}_H. \quad (1)$$

The \mathcal{L}_H loss from the altimeter readings p^{gt} simply aims to minimize the distance from θ at coordinates (p_x^{gt}, p_y^{gt}) to the measured height p_z^{gt} . If we take

$$\Delta^\theta(p) = \theta(p_x, p_y) - p_z \quad (2)$$

to be the signed vertical distance, the averaged loss from one batch of altimeter heights is given by

$$\mathcal{L}_H = \frac{1}{|\{p_j^{gt}\}|} \sum_j \|\Delta^\theta(p_j^{gt})\|. \quad (3)$$

The second part, \mathcal{L}_∇ , aims to reconstruct the ground truth intensity $I_{i,n}$ from the sidescan for each sidescan ping i and each distance bin n ,

$$\mathcal{L}_\nabla = \frac{1}{|\{I_{i,n}\}|} \sum_{i,n} \|\tilde{I}_{i,n} - I_{i,n}\|. \quad (4)$$

The remainder of the paper mainly deals with the difficult problem of estimating the intensities $\tilde{I}_{i,n}$ from the bathymetry θ .

B. Computing seafloor intersections

In a sidescan, the beam width in the longitudinal direction is small enough to mostly be neglected. Spatially, this leaves the reflected volume around a thin arch at a fixed time away from the vehicle. We will refer to such archs as *isotemporal curves*. If we assume an isovelocity *sound velocity profile* (SVP), the isotemporal curve also corresponds to a fixed distance, parameterized by an angle ϕ ,

$$p_{i,n}(\phi) = t_i + d_n R_i [0, \sin(\phi), -\cos(\phi)]^T. \quad (5)$$

While, for simplicity, we assume an isovelocity SVP in this paper, $p_{i,n}$ could in principle be any differentiable

function whose path approximates an isotemporal curve as defined by an SVP.

Additionally, we will assume that the function $\Delta^\theta(p_{i,n}(\phi_k))$ only has one zero-crossing within the interval $[\phi_{min}, \phi_{max}]$. If its derivative is strictly positive around that crossing, we may find it using gradient descent optimization. Such a scheme iteratively updates the angular position ϕ from a starting value $\phi^0 = \frac{1}{2}(\phi_{min} + \phi_{max})$, where ϕ_{min} and ϕ_{max} define the boundaries of the beam,

$$\phi^{k+1} = \phi^k - \frac{\lambda}{d_{i,n}} \frac{d}{d\phi} (\Delta^\theta(p_{i,n}(\phi^k)))^2. \quad (6)$$

The λ parameter describes the update step size, while division by the distance $d_{i,n}$ ensures that the step is comparable across the different curves. We perform a fixed number of gradient descent steps, resulting in the angle $\phi_{i,n}^*$ at the seafloor intersection. If $\phi_{i,n}^* \notin [\phi_{min}, \phi_{max}]$, we exclude it from the loss computation, since no zero-crossing was found within the beam.

C. Lambertian scattering model

Subsequently, we will focus on ways of inferring the model intensity $\tilde{I}_{i,n}$ from the height map model ϕ assuming a Lambertian scattering model. To compute a Lambertian intensity, we first need to define the normal with respect to θ at a point $p \in \mathbb{R}^3$. Given the two gradient components ∇_x, ∇_y it is defined by

$$N^\theta(p) = [-\nabla_x \theta(p_x, p_y), -\nabla_y \theta(p_x, p_y), 1]^T. \quad (7)$$

In the general case, the incident ray of the isotemporal curve $p_{i,n}$ is given by the normal to its path derivative at the point of intersection with the seafloor. Assuming a port-facing sidescan, the rotation from the tangent to the normal is given by the 90° rotation around the x-axis in the sensor frame, $R_i R_x(\frac{\pi}{2}) R_i^T$, giving

$$r_i(\phi) = R_i R_x(\frac{\pi}{2}) R_i^T \frac{d}{d\phi} p_{i,n}(\phi) \quad (8)$$

and specifically, for an isovelocity SVP,

$$\begin{aligned} r_i(\phi) &= d_n R_i R_x(\frac{\pi}{2}) \frac{d}{d\phi} [0, \sin(\phi), -\cos(\phi)]^T \\ &= d_n R_i R_x(\frac{\pi}{2}) [0, \cos(\phi), \sin(\phi)]^T \\ &= d_n R_i [0, -\sin(\phi), \cos(\phi)]^T. \end{aligned}$$

Using N^θ and r_i , we can compute the cosine of the incidence angle, giving the Lambertian scattering contribution $M_{i,n}^\theta$ from one point p . More specifically, we use the \cos^2 approximation, as it is known to give better results at low gracing angles:

$$M_{i,n}^\theta(\phi^*) = \left(r_i(\phi^*)^T N^\theta(p_{i,n}(\phi^*)) \right)^2. \quad (9)$$

D. Beam-pattern, gain and albedo models

In addition to the surface normals implicitly given by the Lambertian intensity, we also estimate other

important parameters of the sensor and its environment. Our full model is inspired by that of Coiras et al. [18]. In addition to the albedo R of the seafloor and the beam-pattern Φ , we also estimate a gain parameter A_i . Each of these parameters are initialized to 1 when training, and are constrained to be positive by passing them through an *exp* function before feeding them into the model. The complete intensity model is given by

$$\tilde{I}_{i,n} = K A_i M_{i,n}^\theta(\phi_{i,n}^*) \Phi(\phi_{i,n}^*) R(p_{i,n}(\phi_{i,n}^*)). \quad (10)$$

Within this context, K is a normalization constant that is estimated once for the whole data set prior to training. While K is there purely to help the optimization converge faster (see Section III-B for details), the rest of the parameters are optimized during training together with θ . The gain parameter A_i is estimated for each sidescan line, and allows for varying gain across the data set. The functions $\Phi(\phi)$ and $R(p)$ are kernel densities whose kernel weights Φ_κ, R_κ are estimated while training. The spread σ of the fixed position kernels are taken to be the range divided by the number of kernels, with $\gamma = \frac{1}{2\sigma^2}$. Thus, the beam-pattern is defined as

$$\Phi(\phi) = \frac{1}{Z} \sum_{\kappa} \Phi_\kappa \exp(-\gamma_\Phi (\phi_\kappa - \phi)^2), \quad (11)$$

while the 2-dimensional albedo function is given by

$$R(p) = \frac{1}{Z} \sum_{\kappa} R_\kappa \exp(-\gamma_R \|x_\kappa - p_{xy}\|^2). \quad (12)$$

Similar to [17], we use a rather coarse approximation of $R_{i,n}$, with only 100 kernels spaced in a grid. This ensures that we do not fit variations appearing only in few sidescan lines, which may be due either to geometry or other factors.

E. Optimization

The proposed representation θ as well as the kernel densities R, Φ are fully differentiable. However, the gradient descent procedure of Equation 6 is not easily differentiable. Instead, for every training batch, we compute the intensity $\tilde{I}_{i,n}$ in Equation 10 from the produced point $p_{i,n}(\phi^*)$, without backpropagating through the gradient descent procedure. As soon as training of the representation θ has converged to be roughly within the true height range, this simplification should have a negligible impact.

With these details out of the way, the loss function of Equation 1 can be optimized with a standard neural network optimizer; in the experiments we use ADAM. Again, it is worth noting the similarities to a differential equation with boundary conditions. The intensity implicitly defines the gradients at some points while the altimeter readings provide the boundary points. For the optimization to converge to a reasonable bathymetry, we have observed that it requires at least some altimeter readings, and preferably at the perimeter.

III. EXPERIMENTS

A. Data set

Our method was evaluated on a data set that also contains high-precision bathymetry that can be used as comparison. The sidescan data was collected using a surface vessel equipped with *RTK GPS*, ensuring high quality positioning. Similar to most AUVs, the sidescan is hull mounted, thus ensuring that its position is accurate as well. Our system takes as input the raw sidescan files produced by the surveys. To facilitate the evaluation of our sidescan modeling, we used the high-precision bathymetry to simulate unambiguous altimeter readings. Since they already agree with the compared bathymetry, this ensures that we evaluate only the effectiveness of our sidescan modeling, thus removing any potential artifacts from an actual altimeter sensor.

Property	Value
Bathymetry res.	0.5m
Sidescan type	Edgetech 4200MP
Sidescan range	0.035s $\Rightarrow \sim 50m$
Sidescan freq.	555kHz
Composition	$\sim 70\%$ Sed. rock, 30% sand
Mean altitude	17m
Survey area	$\sim 350m \times 300m$
Sidescan pings	~ 93000

TABLE II: Data set and survey area characteristics.

When comparing our height map estimate to the high-precision bathymetry, we consider several metrics. Each of them is computed at the native 0.5m scale of the bathymetry. In addition to the mean absolute height difference between the two, we also compare the gradients. The reason for studying the gradients is that the sidescan signal contains information that directly relates to the surface gradients. However, when integrating these gradients to produce the ground truth height map, the estimate will drift. By considering both absolute height and gradients, we can therefore evaluate gradient quality as well as the drift due to integration. The multibeam bathymetry gradient is calculated from finite differences. It is compared both by looking at the cosine similarity to the predicted gradients, as well as the mean absolute gradient magnitude difference.

B. Data preparation

The sidescan signal contains roughly 12000 intensities per head. Our method is able to deal with this high-resolution signal by sampling a lower number of intensities within each training batch. However, a neural bathymetry representation with a reasonable number of parameters is unable to accommodate this level of precision. Moreover, the positioning is most likely not accurate to this level of resolution either. To simplify our analysis, we therefore subsample the signal, keeping only 64 intensities per head in this analysis. Note that

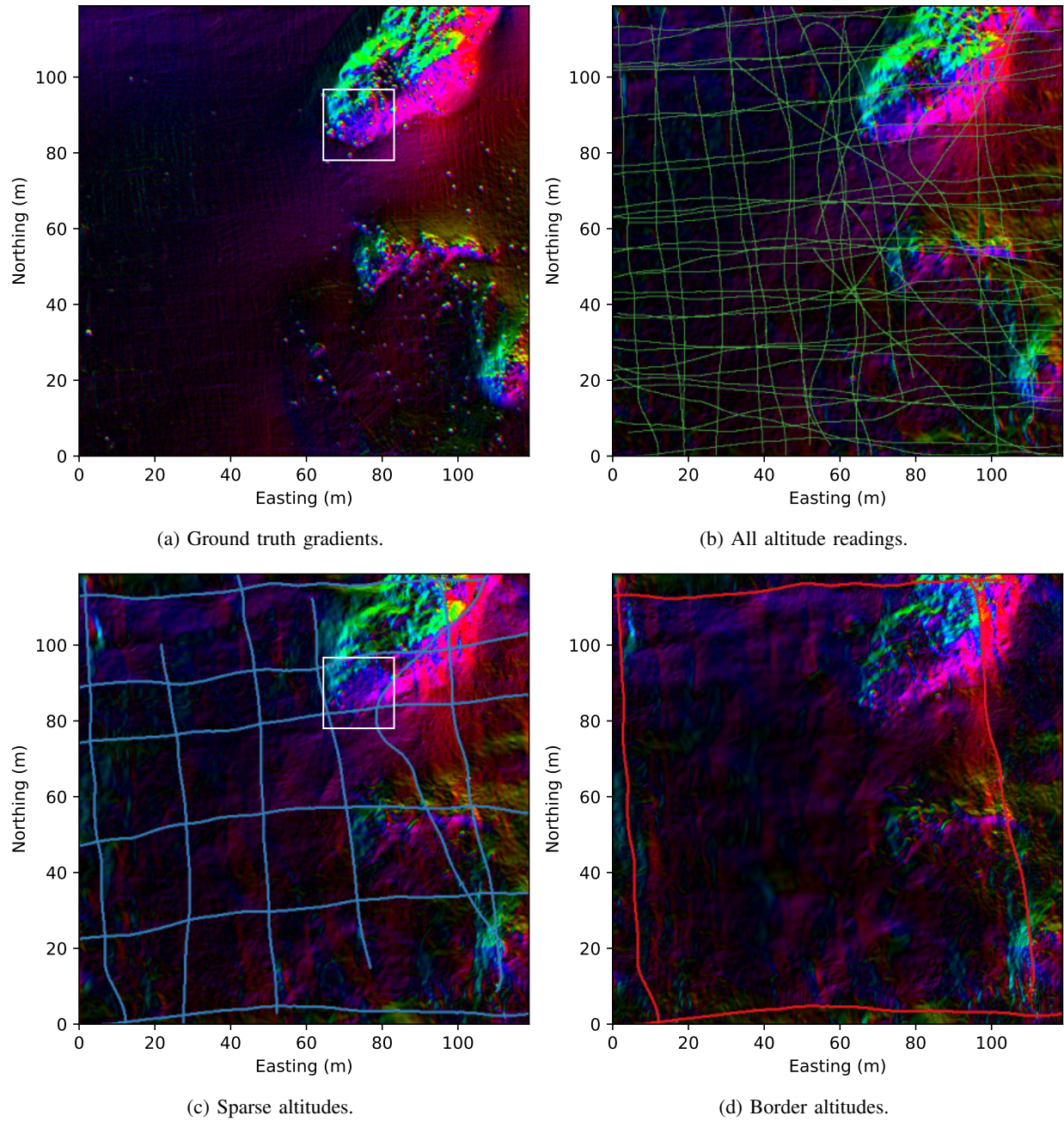


Fig. 3: Height map gradient results with different altimeter reading densities (overlaid lines). On a large scale, when using all or sparse altitude readings, the method manages to reproduce the ground truth bathymetry. With altitudes only at the border of the survey area, the absolute values are not accurate but it still reproduces the general shape of the hills as well as some rocks. Zoomed in example of (a) and (c) (white boxes) can be viewed in Figure 4.

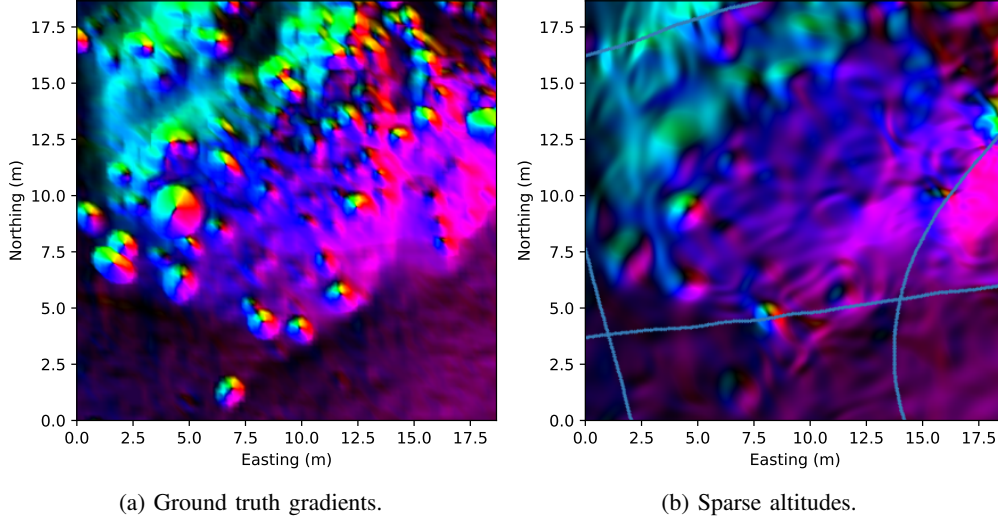


Fig. 4: Zoomed in examples from Figure 3. The model gradients on the right was created from the sparse altimeter readings (blue lines). It manages to reproduce several of the stones not seen in the altimeter data .

the subsampling also aids in filtering out some of the sidescan noise, thus making the training more efficient.

In order to further accelerate the training, we produce a naive estimate of the K normalization parameter from Equation 10 for the whole data set. By assuming a flat seafloor as measured by one altimeter reading below the vehicle, we can produce Lambertian model intensities for the sidescan pings. We then fit K to minimize the distance to the ground truth intensities using a least squares fit on 1% of the pings. The procedure also ensures that the model works to some extent even without learning the A_i , R and Φ parameters.

Since our method only models reflections from the seafloor, any shadows in the waterfall images need to be identified and corresponding data points removed for the training. In our case, we simply remove any intensities below 0.3 after the initial K correction. A more sophisticated scheme may also be applied, such as that of Langer & Hebert[16]. In our specific data set, there were relatively few shadows, and our simple method proved effective at detecting them. Furthermore, we only consider the outer half of the sidescan intensities to avoid any measurements from the nadir area, which typically occupies the first third of the ping.

C. Training

Before feeding into the network, all positional data is scaled by a factor to make sure that all x, y positions are within the range $[-1, 1]$. Since the non-linearity of the network we are using is the sine function, the normalization ensures that the positions can be unambiguously represented by the network.

The network used for the experiments is a multi-layer perceptron with 5 hidden layers, each of width 128. We train the network for 400 epochs, with an initial learning

rate of 2×10^{-4} that is then multiplied by a factor of 0.995 every epoch. Each batch contains 400 sidescan pings and 800 altimeter points. For each ping we sample eight random intensities from each sidescan head, both port and starboard.

IV. RESULTS

We start by investigating reasonable values of some of the main parameters. These results were generated with the full system, including albedo, beam-pattern and gain estimation.

A. Parameter search

In Figure 6 we can see the results of varying the height weight parameters α . Too much emphasis on altimeter readings ($\alpha \gg 1$) seems to result in poor bathymetry estimates. From looking at the produced bathymetries, we conclude that the network focuses too much on the altimeter readings, with a somewhat jagged appearance of the seafloor in between. On the other hand, we also see that the performance drops dramatically as we approach $\alpha = 0$. In this case, the bathymetry seems to disregard altimeter readings, instead producing an overly flat seafloor surface. Since no value seems to significantly outperform $\alpha = 1$ that is what we will use in the remaining experiments.

Next, we investigate the influence of the number of altimeter points in each batch. The number of sidescan points is kept fixed at 400 since that is around the maximum number that can be fed through training without it to slowing down due to the constrained GPU memory bandwidth. In comparison, it is relatively cheap to add more altimeter points. However, as can be seen from Figure 8, there seems to be little gain in supplying

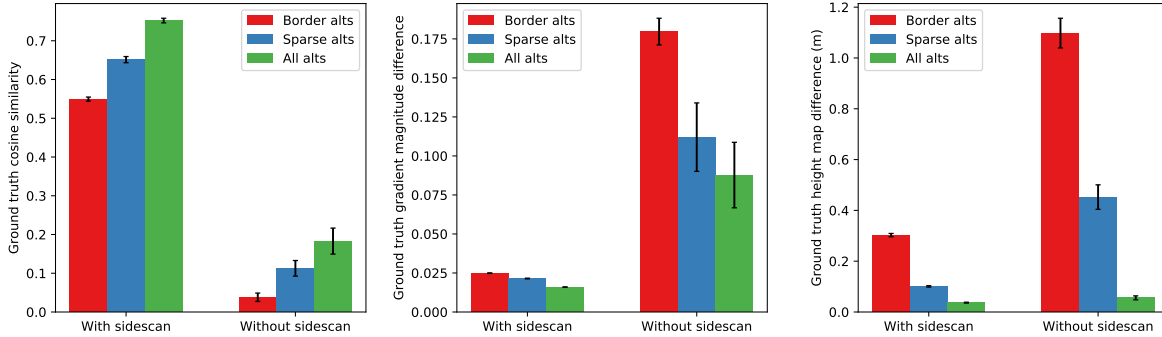


Fig. 5: Comparison of results with and without sidescan as input to the mode, as well as with different altimeter densities. Sidescan improves the quality of the reconstruction significantly in all settings and metrics. The difference is even more pronounced when looking at the gradient quality rather than the absolute height.

more than ~ 500 altimeter points per batch. In the remaining experiments, we use 800 points.

B. No sidescan & Altimeter sparsity analysis

We proceed to investigate the benefit of adding sidescan over just using the sparse altimeter points by themselves. Figure 5 illustrates the improvement, with different altimeter densities. In general, the pure altimeter height maps still look reasonable in the sense that the MLP outputs smooth surfaces in between altimeter points. However, we observe a significant improvement to including the sidescan in the optimization. Interestingly, the improvement is greater when considering the similarity to the gradients rather than the absolute height. This is likely due to the sidescan containing information on the gradient, rather than the height, which may drift when integrating the gradient.

Next, we study the effects of different altimeter densities in detail, by looking at quantitative as well as qualitative results. We choose three scenarios, first with altimeter information for *all* sidescan lines. The resulting gradients are displayed in Figure 3, together with the ground truth bathymetry gradients. The general structure is well approximated, with prominent rocks captured by the reconstruction. While the large-scale gradients are similar, the estimated gradient magnitudes are generally somewhat smaller across the rocks, and many smaller rocks were not identified.

We also test on a *sparse* set containing only 12 lines of altimeter lines, with half of the lines being perpendicular to the other half. Again, looking at Figure 3 we observe a general similarity to the ground truth height map. Compared to the results with all lines, there are are somewhat fewer reconstructed rocks with the sparse lines. However, in the zoomed in example of Figure 4 we can see that the larger rocks are reconstructed in an area away from the altimeter lines. This means those rocks are inferred purely from looking at the sidescan.

In the extreme case of only having lines at the *border* of the survey area, we can also draw similar

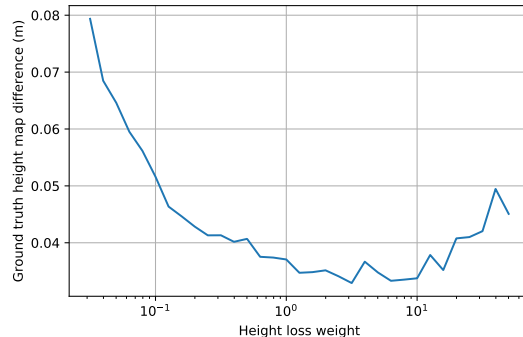


Fig. 6: Mean height map residual as a function of height loss weight α . We observe a minimum around $\alpha = 5$.

conclusions. For example, at the bottom of the hill of Figure 3, we see that the rocks are again reconstructed, this time far away from any altimeter readings. In general, the height map seems to degrade as we include fewer altimeter measurements. However, it maintains a qualitative similarity in between all three densities, with hills and protrusions appearing in the same places, but with different heights. In general, our observations agree with the quantitative results of Figure 5. In summary, the method generates a reasonable estimate even using very few altimeter points at the borders, that then improves the more altimeter points are added. The best result with all altimeter points exhibit an error of around 4cm.

C. Ablation study

In Figure 7 we present the results when omitting estimation of the gain, albedo and beam-pattern parameters. As the gain did not change throughout the mission, it is only natural that estimating a gain for each line did not result in an improvement. Interestingly, it is also not significantly worse than not estimating it, which suggests that the algorithm may be able to handle a

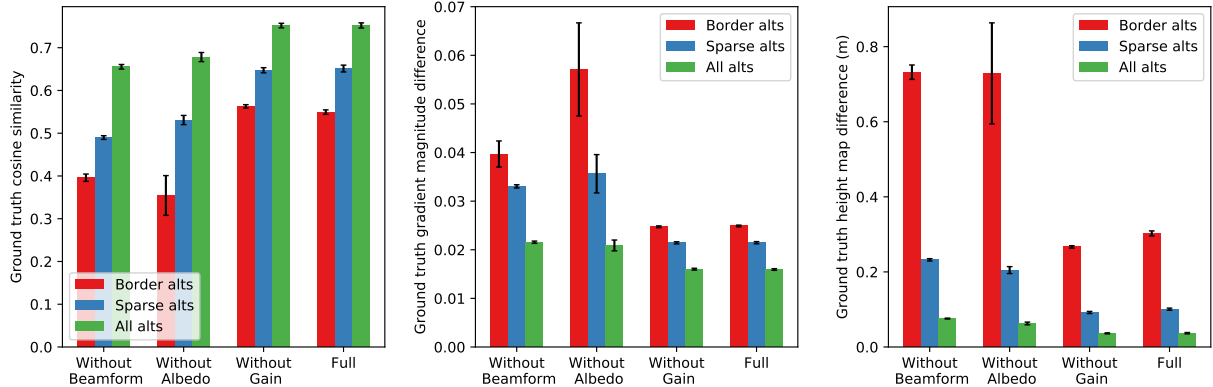


Fig. 7: Ablation study with and without estimating the model parameters, and with different altimeter reading densities. Generally, estimating more parameters results in better estimates, with the largest improvements coming from modeling the beamforms and the seafloor albedo. As may be expected, allowing for variation in intensity in between the lines does not result in an improvement, as the gain remained unchanged throughout the survey.

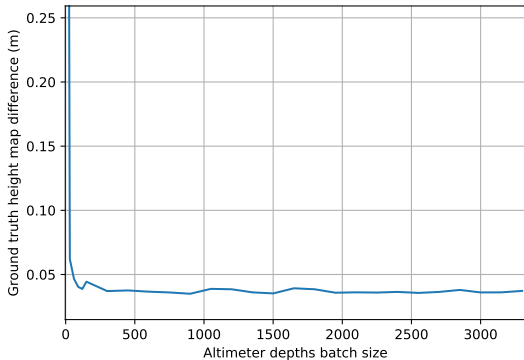


Fig. 8: Mean height map residual as a function of the number of altimeter points in a batch. The training does not benefit significantly from more than ~ 200 points.

varying gain. Both albedo and beam-form estimation present a significant improvement in estimating the height map. This suggests that these two factors play an important role when sensing our environment. It is also clear that they are somewhat orthogonal, since estimating both of them at the same time presents a significant boost. This result also indicates that we had sufficient coverage of the whole area in our data set, thus avoiding overfit in some of the parameters, which would result in poor height map estimates. Looking at Figure 9, we also conclude that the estimates converge to stable values when learnt jointly.

D. Performance

On a computer with an Nvidia GTX 1060, our method is able to compute $\sim 15 \times 10^4$ isotemporal curve intersections per second, and backpropagate the

corresponding intensity losses, along with the altimeter losses. With 400 epochs, this takes about 1h for the given data set containing ~ 93000 pings.

V. CONCLUSIONS

We presented a neural network-based shape-from-shading method that combines sidescan with sparse altimeter readings to build a dense bathymetry height map. In experiments, we demonstrated its ability to fuse sidescan data from a large sidescan survey into a self-consistent bathymetric map. Notably, it was able to infer the positions of rocks that were otherwise only visible in the sidescan. When compared to the ground truth bathymetry from multibeam, the method had an error at the level of centimeters, which is comparable to the error in the multibeam itself. Since the depth profile in between altimeter readings is inferred from the estimated gradient, the estimate sometimes diverges from the true depth. Even when the method exhibited quantitative errors, we found that it gives a valuable qualitative view of the seafloor, clearly indicating the positions of rocks and ridges.

VI. FUTURE WORK

The proposed method is explicitly constructed to take advantage of the superior resolution of the sidescan as compared to other sensors. At a fundamental level, it does not rely on downsampling or discretization. The precision is constrained mainly by the size of the trainable network, the positioning accuracy, and the aperture of the sensor. In theory, if the aperture can be modeled within this framework, and if the positioning error could be mitigated, the model could achieve super-resolution bathymetry.

In practice, the necessary positioning accuracy can not be achieved at this point, since only the slightest deviation in angle leads to a significant change in the

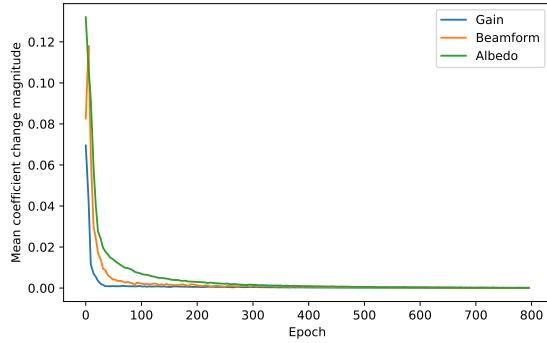


Fig. 9: Mean absolute change of the estimated parameters in between epochs. All parameters have mostly converged around epoch ~ 300 .

outer parts of the sidescan ping. A tantalizing prospect would therefore be to also optimize the sidescan poses together with the bathymetry. Since the model is fully differentiable, this is possible, but great care has to be taken for the optimization to still be constrained. In our minds, an obvious first foray is to optimize the sidescan pose with respect to the vehicle’s navigation frame.

With improved position estimates, it would also be possible to combine sidescan with a multibeam survey. As discussed, the current method may not reproduce absolute depths accurately everywhere. If we could use dense multibeam measurements to fix the height map in more places, that problem may be alleviated. With sufficiently accurate sidescan positions, our method may be able to enable resolve smaller details than is currently possible, while maintaining the same precision as in the coarser multibeam bathymetry.

VII. ACKNOWLEDGMENTS

This work was partially supported by the Wallenberg AI, Autonomous Systems and Software Program (WASP), by the Stiftelsen för Strategisk Forskning (SSF) through the Swedish Maritime Robotics Centre (SMaRC) (IRC15-0046), and by VINNOVA, project number 2020-04551. Our data set was acquired in collaboration with Marin Mätteknik (MMT) Gothenburg.

REFERENCES

- [1] J. M. Bell, M. J. Chantler, and T. Wittig, “Sidescan sonar: a directional filter of seabed texture?,” *IEEE Proceedings-Radar, Sonar and Navigation*, vol. 146, no. 1, pp. 65–72, 1999.
- [2] E. Coiras, Y. Petillot, and D. M. Lane, “An expectation-maximization framework for the estimation of bathymetry from side-scan sonar images,” in *Europe Oceans 2005*, vol. 1, pp. 261–264, IEEE, 2005.
- [3] B. Mildenhall, P. P. Srinivasan, M. Tancik, J. T. Barron, R. Ramamoorthi, and R. Ng, “Nerf: Representing scenes as neural radiance fields for view synthesis,” in *ECCV*, 2020.
- [4] V. Sitzmann, J. N. Martel, A. W. Bergman, D. B. Lindell, and G. Wetzstein, “Implicit neural representations with periodic activation functions,” in *Proc. NeurIPS*, 2020.
- [5] J. Yan, J. Meng, and J. Zhao, “Real-time bottom tracking using side scan sonar data through one-dimensional convolutional neural networks,” *Remote sensing*, vol. 12, no. 1, p. 37, 2020.
- [6] Y. Xie, N. Bore, and J. Folkesson, “Inferring depth contours from sidescan sonar using convolutional neural nets,” *IET Radar, Sonar & Navigation*, vol. 14, no. 2, pp. 328–334, 2019.
- [7] K. L. Williams and D. R. Jackson, “Bistatic bottom scattering: Model, experiments, and model/data comparison,” *The Journal of the Acoustical Society of America*, vol. 103, no. 1, pp. 169–181, 1998.
- [8] J. M. Bell and L. M. Linnett, “Simulation and analysis of synthetic sidescan sonar images,” *IEEE Proceedings - Radar, Sonar and Navigation*, vol. 144, pp. 219–226, Aug 1997.
- [9] E. Durá, J. Bell, and D. Lane, “Reconstruction of textured seafloors from side-scan sonar images,” *IEEE Proceedings-Radar, Sonar and Navigation*, vol. 151, no. 2, pp. 114–126, 2004.
- [10] E. Coiras, A. Ramirez-Montesinos, and J. Groen, “Gpu-based simulation of side-looking sonar images,” in *OCEANS 2009-EUROPE*, pp. 1–6, May 2009.
- [11] Y. Pailhas, Y. Petillot, C. Capus, and K. Brown, “Real-time sidescan simulator and applications,” in *OCEANS 2009-EUROPE*, pp. 1–6, May 2009.
- [12] J. Folkesson, H. Chang, and N. Bore, “Lambert’s cosine law and sidescan sonar modeling,” in *2020 IEEE/OES Autonomous Underwater Vehicles Symposium (AUV)*, pp. 1–6, 2020.
- [13] N. Bore and J. Folkesson, “Modeling and simulation of sidescan using conditional generative adversarial network,” *IEEE Journal of Oceanic Engineering*, vol. 46, no. 1, pp. 195–205, 2021.
- [14] B. K. Horn, “Obtaining shape from shading information,” *The psychology of computer vision*, pp. 115–155, 1975.
- [15] R. J. Woodham, “Photometric method for determining surface orientation from multiple images,” *Optical engineering*, vol. 19, no. 1, p. 191139, 1980.
- [16] D. Langer and M. Hebert, “Building qualitative elevation maps from side scan sonar data for autonomous underwater navigation,” in *Proceedings. 1991 IEEE International Conference on Robotics and Automation*, pp. 2478–2483 vol.3, April 1991.
- [17] A. E. Johnson and M. Hebert, “Seafloor map generation for autonomous underwater vehicle navigation,” *Autonomous Robots*, vol. 3, no. 2-3, pp. 145–168, 1996.
- [18] E. Coiras, Y. Petillot, and D. M. Lane, “Multiresolution 3-d reconstruction from side-scan sonar images,” *IEEE Transactions on Image Processing*, vol. 16, pp. 382–390, Feb 2007.
- [19] J. Cuschieri and M. Hebert, “Three-dimensional map generation from side-scan sonar images,” 1990.
- [20] K. Bikonis, A. Stepnowski, and M. Moszynski, “Computer vision techniques applied for reconstruction of seafloor 3d images from side scan and synthetic aperture sonars data,” *Journal of the Acoustical Society of America*, vol. 123, no. 5, p. 3748, 2008.
- [21] P. Woock and J. Beyerer, “Seafloor shape estimation by ray-traced kernels,” in *OCEANS 2014-TAIPEI*, pp. 1–8, IEEE, 2014.
- [22] K. R. Jones and P. Traykovski, “A method to quantify bedform height and asymmetry from a low-mounted sidescan sonar,” *Journal of Atmospheric and Oceanic Technology*, vol. 35, no. 4, pp. 893–910, 2018.
- [23] Rongxing Li and Sunny Pai, “Improvement of bathymetric data bases by shape from shading technique using side-scan sonar images,” in *OCEANS 91 Proceedings*, vol. 1, pp. 320–324, 1991.
- [24] B. Horn, B. Klaus, and P. Horn, *Robot vision*. MIT press, 1986.
- [25] P. Woock, “Deep-sea seafloor shape reconstruction from side-

scan sonar data for auv navigation,” in *OCEANS 2011 IEEE-Spain*, pp. 1–7, IEEE, 2011.

- [26] J. Zhao, X. Shang, and H. Zhang, “Reconstructing seabed topography from side-scan sonar images with self-constraint,” *Remote Sensing*, vol. 10, no. 2, p. 201, 2018.
- [27] T. A. Huang and M. Kaess, “Towards acoustic structure from motion for imaging sonar,” in *2015 IEEE/RSJ International Conference on Intelligent Robots and Systems (IROS)*, pp. 758–765, IEEE, 2015.
- [28] N. Brahim, D. Guériot, S. Daniel, and B. Solaiman, “3d reconstruction of underwater scenes using didson acoustic sonar image sequences through evolutionary algorithms,” in *OCEANS 2011 IEEE-Spain*, pp. 1–6, IEEE, 2011.
- [29] M. D. Aykin and S. Negahdaripour, “Forward-look 2-d sonar image formation and 3-d reconstruction,” in *2013 OCEANS-San Diego*, pp. 1–10, IEEE, 2013.
- [30] M. D. Aykin and S. Negahdaripour, “Three-dimensional target reconstruction from multiple 2-d forward-scan sonar views by space carving,” *IEEE Journal of Oceanic Engineering*, vol. 42, no. 3, pp. 574–589, 2017.
- [31] E. Westman and M. Kaess, “Wide aperture imaging sonar reconstruction using generative models,” in *2019 IEEE/RSJ International Conference on Intelligent Robots and Systems (IROS)*, pp. 8067–8074, IEEE, 2019.
- [32] E. Westman, I. Gkioulekas, and M. Kaess, “A volumetric albedo framework for 3d imaging sonar reconstruction,” in *2020 IEEE International Conference on Robotics and Automation (ICRA)*, pp. 9645–9651, IEEE, 2020.
- [33] T. Guerneve, K. Subr, and Y. Petillot, “Three-dimensional reconstruction of underwater objects using wide-aperture imaging sonar,” *Journal of Field Robotics*, vol. 35, no. 6, pp. 890–905, 2018.
- [34] T. M. Marston and J. L. Kennedy, “Volumetric acoustic imaging via circular multipass aperture synthesis,” *IEEE Journal of oceanic engineering*, vol. 41, no. 4, pp. 852–867, 2016.
- [35] M. Tancik, P. P. Srinivasan, B. Mildenhall, S. Fridovich-Keil, N. Raghavan, U. Singhal, R. Ramamoorthi, J. T. Barron, and R. Ng, “Fourier features let networks learn high frequency functions in low dimensional domains,” *NeurIPS*, 2020.



John Folkesson received the B.A. degree in physics from Queens College, City University of New York, New York, NY, USA, in 1983, and the M.Sc. degree in computer science, and the Ph.D. degree in robotics from Royal Institute of Technology (KTH), Stockholm, Sweden, in 2001 and 2006, respectively. He is currently an Associate Professor of robotics with the Robotics, Perception and Learning Lab, Center for Autonomous Systems, KTH. His research interests include navigation, mapping, perception, and situation awareness for autonomous robots.



Nils Bore received the M.Sc. degree in mathematical engineering from the Faculty of Engineering, Lund University, Lund, Sweden, in 2012, and the Ph.D. degree in computer vision and robotics from the Robotics Perception and Learning Lab, Royal Institute of Technology (KTH), Stockholm, Sweden, in 2018. He is currently a researcher with the Swedish Maritime Robotics (SMaRC) project at KTH. His research interests include robotic sensing and mapping, with a focus on probabilistic reasoning and inference. Most of his recent work has been on applications of specialized neural networks to underwater sonar data. In addition, he is interested in system integration for robust and long-term robotic deployments.